Long-term Hematopoietic Stem Cells as Sanctuary Niche during Treatment Failure in Visceral Leishmaniasis

Laura Dirkx
University of Antwerp https://orcid.org/0000-0002-1020-466X
Sarah Hendrickx
University of Antwerp
Louis Maes
University of Antwerp https://orcid.org/0000-0002-2324-9509
Guy Caljon (Guy.Caljon@uantwerpen.be)
University of Antwerp https://orcid.org/0000-0002-4870-3202

Article

Keywords: visceral leishmaniasis, bone marrow, post-treatment relapse

Posted Date: March 10th, 2021

DOI: https://doi.org/10.21203/rs.3.rs-261107/v1

Abstract

The increasing frequency of treatment failure in visceral leishmaniasis (VL) has already resulted in discontinuation of various first-line drugs. Although most studies focus on associations with parasitic drug resistance, a knowledge gap remains about other factors determining cure versus relapse. The present study used double bioluminescent/fluorescent *Leishmania infantum* and *L. donovani* reporter lines to study relapse at the tissue and cellular level. In combination with 123 different treatments in golden Syrian hamsters, the observations provide evidence of parasites surviving in the bone marrow (BM), identifying this tissue as a sanctuary site from where the host can be recolonized. Long-term hematopoietic stem cells (LT-HSC; Lin- Sca1 + cKit + CD48- CD150+) were found to become readily infected through invasion rather than phagocytosis. Compared to other BM cells and macrophages, LT-HSCs constitute a hospitable cellular niche with low nitric oxide and reactive oxygen species levels and harbouring enormous parasite burdens. Moreover, we found that infected LT-HSCs are less sensitive to antileishmanial reference drugs in comparison to macrophages. Given the important clinical implications for the current field situation of increasing post-treatment relapse rates, this study represents an essential step by identifying the BM cellular niches responsible for *Leishmania* persistence and treatment failure.

Introduction

Visceral leishmaniasis (VL) is a lethal neglected tropical disease caused by the obligate intracellular protozoan *Leishmania* [1, 2] and transmitted through the bites of infected phlebotomine sand flies [3, 4]. In the vertebrate host, parasites propagate as amastigotes in monocyte-derived cells of the liver, spleen and bone marrow (BM) and eventually cause life-threatening complications [5-7].

Successful curative treatment of VL is notoriously challenging. A particularly alarming situation in the Mediterranean basin is the increasing number of *L. infantum* infections that are not adequately responding to any of the known antileishmanial drugs [8]. To date, antimony (Sb) and miltefosine (MIL) monotherapy against VL have been discontinued in the Indian subcontinent [9]. In general, treatment failure occurs frequently and treatment options could become critically compromised [10]**.** Associations are often sought with drug resistance, although microorganisms can also be impervious to drugs without selection of genetic mutations. The formation of viable non-replicating cells, also known as persister-like cells, is common among bacteria and has also been described for *Plasmodium falciparum* and *P. vivax*, *Toxoplasma gondii*, *Trypanosoma cruzi, Leishmania* spp. and *Mycobacterium tuberculosis* [11]. Persistent infections can occur in many different tissues and cells throughout the host, such as hepatocytes (*P. vivax*), skeletal muscle and neurons (*T. gondii*), adipose tissue (*T. cruzi*) and the BM (*M. tuberculosis*) [12-16]. Some of these niches give protection against active immunity and drug action [11]. Within the BM, VL parasites are renowned to induce emergency hematopoiesis with consequent exhaustion of hematopoietic stem cells (HSC) [17-19] and induce leucopenia, neutropenia, thrombocytopenia and anemia [20]. While the long-term HSC (LT-HSC) are normally in a quiescent state, infection drives these cells into active proliferation with a reduction of self-renewal capacity, leading to defects in blood homeostasis [21, 22].

Our historical laboratory data triggered the hypothesis that treatment is generally less effective in the BM, representing a reservoir site from where relapse can occur. To date, *Leishmania* spp. have been extensively reported to reside primarily within macrophages and dendritic cells [23], and case studies illustrate infested macrophages on BM aspirates [24-26]. However, the exact pre- and post-treatment tropism in the BM has not yet been exhaustively described. In this study, LT-HSC were found to become more readily infected and to display an increased tolerance to a range of antileishmanial drugs. This indicates that infection of LT-HSCs may not only allow escape from the host immune response but also from antileishmanial drug action. Our results further demonstrate a change in the functional profile of these infected stem cells, specifically a decrease in reactive oxygen species (ROS) and nitric oxide (NO) levels, of which the latter is described as one of the most important effector molecules involved in parasite killing [27]. In summary, this study identified a protective cellular niche of persistent *Leishmania* parasites in the BM. Given the current field situation of increasing post-treatment relapse rates, this aspect should become a requisite to advanced pharmacodynamic and novel drug exploration.

Results

1. **Bone marrow as a niche for persistent VL parasites**

By means of *in vivo* bioluminescence imaging (BLI), we developed a reproducible post-treatment relapse model in BALB/c mice using sub-curative PMM treatment. After 5 consecutive days of 350 mg/kg *s.i.d.* intraperitoneal (i.p.) injections of PMM, a significant decrease of parasite burdens in the liver, spleen and BM was obtained (Fig. 1A), indicating that the drug is able to reach all these infection sites. However, low-level BM burdens remained at the end of treatment 2 weeks post-infection (wpi) as evidenced by imaging at a high sensitivity scale (Fig. 1B). In the absence of drug pressure, these burdens re-emerged, indicating that BM represents a niche where parasites can survive antileishmanial treatment. Subsequently, parasites appear able to recolonize target organs with BLI signals increasing from 4-5 wpi onwards in the spleen, but not in the liver (Fig. 1C). Besides the BALB/c model, the golden Syrian hamster model of symptomatic progressive VL was also used as it is considered more representative for human VL and studying drug efficacy and relapse. Own historical laboratory data in the early curative VL hamster model using diverse experimental compounds and reference drugs revealed that the BM was indeed the most difficult to clear. In extreme cases, no drug activity was recorded in the BM at all (Fig. 1D).

2. **Identification of specific BM cell niches for viable *Leishmania* parasites during infection and after relapse**

To identify the specific BM cell subsets in which the parasites reside while simultaneously confirming parasite viability, a promastigote back-transformation assay [28] was performed on sorted stem cells and progenitors according to their specific markers (Fig. 2A). Additionally, Giemsa staining was performed on these cells to visualize infection. For this, both infected and relapsed mice were used at 6 wpi (5 weeks after treatment) in which it was shown that a proportion of long-term hematopoietic stem cells (LT-HSC) and multipotent progenitors 2 (MPP2) harbour viable parasites during a regular infection and after

relapse (Fig. 2B). The presence of amastigotes was confirmed by Giemsa staining which also revealed that LT-HSCs harboured more parasites than MPP2s (Fig. 2C).

3. **LT-HSCs are exceptionally susceptible host cells to VL infection**

Progenitor and stem cells only represent 0.01% of the total BM, hence requiring enrichment for analysis in the complex pool of BM cellular constituents [29]. The lineage positive and negative cells were separated using negative magnetic sorting prior to *ex vivo* infection. Sorted cells were co-cultured with metacyclic *L. infantum* (LEM3323 WT$^{PpyRE9/DsRed}$) promastigotes for 24, 48 and 72 hours, followed by flow cytometry analysis. Compared to the various BM cell subsets, LT-HSCs (Lin- Sca1+ cKit+ CD48- CD150+) were readily infected with *Leishmania*, both in terms of proportion of infected cells (% of infection) and number of parasites per cell based on the DsRed median fluorescence intensity (MFI) (Fig. 3A). Interestingly, the MFI of infected LT-HSCs increased over time compared to T_0 (24 hpi) implying that these cells are highly permissive for amastigote multiplication, in contrast to parasite burdens in infected MPP2 cells which seemed to stagnate (Fig. 3B). Compared to established host cells for *Leishmania*, *i.e.* BM-derived macrophages and dendritic cells, LT-HSC infection rates were lower whereas the median fluorescence intensity was substantially higher, representative for substantially higher intracellular burdens (Fig. 3C). Strikingly high amastigote burdens in LT-HSCs were revealed using Giemsa and immunofluorescence analyses post sorting (Fig. 3D and E) and also after using *L. donovani* Ldl82 WT$^{PpyRe9/DsRed}$ strain (supplementary Fig. S1).

4. ***Leishmania* infection of LT-HSCs is established through invasion rather than phagocytosis and alters their functional profile**

It has been described that stem cells reside in the immune privileged niche of the BM, guarded by regulatory T cells [30]. It is unknown whether hematopoietic stem cells have the capacity to phagocytize parasitic organisms. *Leishmania* are obligate intracellular protozoa that are mainly taken up by phagocytes [31], therefore we explored the possibility of parasite engulfment by LT-HSCs by comparing the entry of live and fixed parasites in LT-HSCs and BM-derived macrophages. Following a 2-hour co-incubation, we observed that both macrophages and LT-HSCs became infected with live parasites whereas only macrophages phagocytized paraformaldehyde fixed parasites (Fig. 4A). To further substantiate these results, parasites were conjugated to pH-sensitive pHrodo dye to specifically detect phagocytosis in live cells whereby the same observation was made, *i.e.* entry into LT-HSCs requires live parasites indicating involvement of active invasion rather than phagocytic processes.

To evaluate the impact of infection on HSC functionality, the production of oxidative radicals as antiparasitic response was examined using flow cytometry. From 24 hours of *ex vivo* infection onwards, intracellular NO and ROS levels notably declined in DsRed+ LT-HSCs compared to naive cells or DsRed- cells within the same well (Fig. 4B, top). In contrast, NO and ROS levels were elevated or stable in infected macrophages (Fig. 4B, bottom).

5. **Infected LT-HSCs show enhanced tolerance to antileishmanial reference drug action compared to macrophages**

To understand the privileged cellular niche that LT-HSCs may represent for *Leishmania* parasites, their sensitivity was tested using the antileishmanial reference drugs PMM, MIL and SSG. Sorted LT-HSCs and BM-derived macrophages were infected and exposed for 120 h to the various drugs at two concentrations, selected based on previous research [32]. In comparison to macrophages, LT-HSCs exhibit an enhanced tolerance to PMM, MIL and SSG both during *L. donovani* (Fig. 5A) and *L. infantum* (Fig. 5B) infection. As seen in figure 3, parasite burdens in LT-HSCs are much higher than in macrophages and higher drug concentrations are required. These observations show that LT-HSCs are indeed very permissive host cells that support post-treatment survival of the intracellular parasites.

Discussion

Many infectious diseases suffer from post-treatment clinical reactivation, and protective tissues or cellular niches have gained increasing awareness in the last couple of years. A well-known example is the liver that can be colonized by dormant or hypnozoite stages of *P. vivax*. These stages are less susceptible for antimalarial therapies and can reactivate [15, 33]. The adipose tissue has been described as a hiding place for *Trypanosoma* species, which may be less amenable for drug treatment due to a low tissue perfusion rate [14]. In the present study, the importance of the BM as a relapse-prone niche during VL was unveiled. The possibility of the BM as sanctuary site was already indicated in 2014 by a rare clinical case of VL after allogeneic BM transplantation from an asymptomatic Portuguese donor [25]. Parasite replication at systemic sites such as the BM is characteristic for the progressive disease course of VL. Chronic *L. donovani* infection studies in mice revealed that emergency hematopoiesis is induced, a stress response that activates HSCs and results in hematological alterations [17]. Besides *Leishmania*, the BM was identified as an antibiotic-protective niche for *M. tuberculosis* where it was shown that *Mtb* can infect CD271+ BM MSCs *in vitro* and *in vivo* in the presence or absence of antibiotic pressure [34]. It was also demonstrated that even after prolonged treatment, *Mtb* survived in CD271+ MSCs [16]. Apart from MSCs, presence of *Mtb* in LT-HSCs has been documented in human and mouse latent TB infections [35].

HSCs are progenitor cells that continuously replenish all blood cell types through a series of differentiation steps and repeated cell divisions. These cells can be classified in two subsets according to their long-term or short-term self-renewal capacity. Long-term HSCs (Lin-Sca1+cKit+CD48−CD150+) can regenerate over a longer period of time and will subsequently differentiate into short-term HSCs (Lin-Sca1+cKit+CD48−CD150−) and multipotent progenitors (MPP2: Lin-Sca1+cKit+CD48+CD150+ and MPP3/4: Lin-Sca1+cKit+CD48+CD150−). MPPs lack self-renewal capacity but can further differentiate in lineage committed cells such as common lymphoid progenitors (CLP) or common myeloid progenitors (CMP). MPP2s mostly give rise to pre-megakaryocyte-erythroid progenitors (PreME) and pre-megakaryocyte progenitors (PreMeg), whereas MPP3/4 cells differentiate into CMPs and granulocyte-monocyte progenitors (GMP) [36-39]. MSCs (CD90.2+CD105+CD271+) are distinct from HSCs as they

shape the BM stroma by differentiating in adipocytes, osteoblasts, osteoclasts, mast cells, fibroblasts, endothelial cells and smooth muscle cells [40].

LT-HSCs reside in the immune privileged niche of the BM and have been characterized as relatively quiescent stem cells (in the G0 phase of cell cycle) with the capacity of self-renewal [29, 30, 41]. During VL infection, most LT-HSCs were found to have entered cell cycle (G0 to G1) correlating with functional exhaustion. More specifically, HSCs were skewed to differentiate into non-classical myeloid progenitors with a regulatory suppressor cell-like phenotype that is more permissive to parasite infection [19]. Modification of the host's BM emergency response thus enables *Leishmania* to promote its own proliferation and allows continued infection. Lopes *et al*. [42] recently described that *L. infantum* is capable to infect CD45+ BM cells and CD271+CD45- MSCs *in vitro* and *in vivo*. The authors further confirmed the parasite's viability highlighting the importance of the BM stroma during VL infection. A study by Carvalho-Gontijo *et al.* [43] also documented the presence of *L. infantum* in human CD34+ stem cells. Our study further pinpointed the exact cellular tropism in the various stem cell and progenitor subsets. Parasite loads differed substantially in these cell types with single parasites in BM monocytes whereas macrophages and myeloblasts can harbor multiple [19]. In our study, LT-HSCs were surprisingly found to accommodate excessive burdens of parasites. It has indeed been described that some intrinsic properties of stem cells may provide opportunities for the pathogen to evade immune responses and drug action, *e.g.* by avoiding the induction of cytotoxic T cell responses and by enhanced drug efflux [29, 42].

Our observation of the vast numbers of intracellular amastigotes may also explain the observed lower drug responsiveness. Based on a large *in vivo* drug evaluation effort (Fig. 1D) that we conducted in the frame of a collaboration with the Drugs for Neglected Disease *initiative* (DND*i*), drug discovery activities should preferably consider this particular BM niche during early discovery phase. Drugs with favorable pharmacokinetic properties to target the BM could potentially be more efficient in targeting the LT-HSC burdens, whereas other compounds may only be effective in organs such as the liver and spleen and be less secure of post-treatment relapse.

Besides the implications for drug discovery, the fundamental biology of the parasite interaction with these cells deserves further exploration. The particular tropism in BM for LT-HSCs was not related to phagocytosis as we found that these cells are unable to engulf VL parasites. *Leishmania* is well established to infect non-phagocytic cells, such as fibroblasts [44], keratinocytes [45], and hepatocytes [46]. Although the invasion mechanisms for non-phagocytic cells are poorly understood, diverse mechanisms may be implicated [31]. Several molecules are involved in the internalization of *Leishmania* parasites [47], but dditional research will be needed to understand *Leishmania* entry into LT-HSCs. Multi-omics profiling of infected LT-HSCs and the intracellular parasites in envisaged to further elucidate the host-parasite interactions in this particular cellular niche [48].

LT-HSCs support extensive intracellular amastigote multiplication that is significantly more pronounced than in macrophages. The production of reactive oxygen and nitrogen species is a prominent and thoroughly regulated antileishmanial response of macrophages aimed at killing the parasite without

damaging the host cell. These oxidative mechanisms are in part stimulated by phagocytosis and involve various signaling and effector molecules. NO is one of the major reactive species in macrophages produced by inducible nitric oxide synthase (iNOS) [49] which mediates intracellular killing of *Leishmania* [27]. The effects of ROS are variable amongst *Leishmania* species: some are susceptible to their action (*L. donovani* [50], *L. major* [51]), while others appear resistant (*L. guyanensis* [52], *L. amazonensis* [53]). Interestingly, our experiments demonstrate substantially decreased levels of both NO and ROS in infected LT-HSCs, creating a more hospitable environment for parasite survival and multiplication. Balanced ROS levels are known to be pivotal for naive LT-HSCs to maintain stem cell function and hematopoietic homeostasis. Stem cells in the BM also reside in a relatively hypoxic environment where low ROS and NO levels sustain a quiescent state and support self-renewal capacity [54]. In the event of ROS induction, stem cell differentiation is triggered and can lead to HSC exhaustion [55]. Similarly, NO stimulation induces the expansion of HSCs and commitment to the myeloid progeny [56].

In summary, the BM and particularly the LT-HSCs were identified as a protective niche during drug treatment in visceral leishmaniasis. The decreased levels of both ROS and NO in infected LT-HSCs could participate in the underlying basis for the observed excessive intracellular parasite burdens. Besides the fundamental insights into the cellular interactions, drug discovery efforts will need to be tweaked to be effective against parasites residing in this newly identified highly permissive host cell.

Methods

Leishmania parasites

The *L. infantum* strain MHOM/FR/96/LEM3323, with an inherent Sb resistance, was obtained from a HIV-positive patient from the Languedoc area in Southern France and kindly provided by CNRL (Montpellier, France). The *L. donovani* strain MHOM/ET/67/L82 was isolated from an Ethiopian VL-patient. Both were modified to express bioluminescent (PpyRE9) and/or fluorescent (DsRed) reporter proteins (LEM3323 WT^{PpyRE9}, LEM3323 WT$^{PpyRE9/DsRed}$ and Ldl82 WT$^{PpyRE9/DsRed}$). Promastigotes were sub-cultured twice weekly at 25°C in hemoflagellate-modified minimal essential medium (HOMEM, Gibco®), supplemented with 10 % inactivated fetal calf serum (iFCS), 200 mM L-glutamine, 16.5 mM $NaHCO_3$, 40 mg/L adenine, 3 mg/L folic acid, 2 mg/L D-biotin and 2.5 mg/L hemin. The number of passages were kept as low as possible to maintain parasite virulence.

Laboratory animals

Female BALB/c mice (6-8 weeks old) were purchased from Janvier (Genest-Saint-Isle, France) and accommodated in individually ventilated cages in pathogen-free conditions. They were provided with food for laboratory rodents (Carfil, Arendonk, Belgium) and water *ad libitum*. Euthanasia was performed in CO_2 chambers followed by cervical dislocation, and tissues were collected under aseptic conditions. The use of laboratory rodents was carried out in strict accordance to all mandatory guidelines (EU directives, including the Revised Directive, 2010/63/EU on the Protection of Animals used for Scientific

Purposes that came into force on 01/01/2013, and the declaration of Helsinki in its latest version) and was approved by the Ethical Committee of the University of Antwerp, Belgium (UA-ECD 2019–04). Animals were subdivided in experimental groups based on simple randomization. Mice were kept in quarantine for at least 5 days before infection.

Primary mouse cells

Mouse BM was collected from BALB/c mice using two distinct techniques, based on pilot studies comparing alternative methods in terms of yield and quality. For both techniques, mice were sacrificed, and hind legs aseptically removed. Isolated femurs and tibias were cleaned by removing soft tissue from the bone using 70% ethanol-soaked cloth and tweezers.

For the crushing technique, the protocol was adapted from Lo Celso and Scadden [57]. Briefly, bones were crushed with mortar and pestle in ammonium-chloride-potassium (ACK) buffer (0.15 M NH_4Cl, 1.0 mM $KHCO_3$, 0.1 mM Na_2EDTA) for erythrocyte lysis. Single cell suspensions were obtained by filtering through MACS® SmartStrainers (100 µm, Miltenyi Biotec), centrifuged at 500×*g* for 10 min (4°C) and resuspended in phosphate-buffered saline (PBS) + 0.2% FCS. For efficient depletion of mature lineage-positive hematopoietic cells and to specifically isolate the preferred lineage-negative cells (*i.e.* undifferentiated progenitor cells), the Direct Lineage Cell Depletion Kit (Miltenyi Biotec) was employed according to manufacturer's instructions. Following lineage depletion, cells were counted in PBS and resuspended in PBS + 0.2% bovine serum albumin (BSA) buffer to 2×10^7 cells/mL. Cells were kept on ice during all procedures.

The centrifugation method was adjusted from the protocol described by Amend *et al.* [58] and Dobson *et al.* [59]. Briefly, a 0.5 mL microcentrifuge tube was perforated at the bottom with a 21G needle and nested inside a 1.5 mL tube (both from Eppendorf). After collection of femurs and tibias, one proximal end (knee epiphysis) was cut-off and placed in the 0.5 mL tube. Nested tubes were centrifuged in a microcentrifuge at 10,000×*g* for 15 sec. Both long bones appeared white and a large visual pellet was observed in the 1.5 mL tube. This pellet was then resuspended in ACK buffer for erythrocyte lysis.

To obtain BM-derived macrophages (BMDM), cells were centrifuged at 500×*g* for 10 min at 4°C, resuspended in Roswell Park Memorial Institute (RPMI) medium (Gibco®) and divided over Petri dishes (Starstedt) supplemented with BM medium [RPMI 1640 medium with 10% (v/v) iFCS, 1% non-essential amino acids (NEAA), 1% sodium pyruvate, 1% L-glutamine, 50 U/mL penicillin, 50 µg/mL streptomycin (all from Gibco®) and 15% L929 supernatant with M-CSF]. Following a 6-day incubation at 37°C with 5% CO_2, the macrophages were collected by replacing the BM medium with ice cold dissociation buffer [PBS with 1% 0.5 M ethylenediaminetetraacetic acid (EDTA) and 2% 1 M 4-(2-hydroxyethyl)-1-piperazine-ethanesulfonic acid (HEPES)]. After detachment, the macrophage cell suspension was centrifuged at 500×*g* for 10 min and resuspended in RPMI medium. The number of macrophages was counted in PBS using a KOVA® counting chamber. Cells were seeded in a 96-well plate (3×10^4 cells/well) or a 24-well plate ($1x10^6$ cells/well) and incubated for 24 h at 37°C with 5% CO_2 to allow adherence of the BMDMs.

To differentiate BM cells into dendritic cells, cells were cultured in Petri dishes in DC medium [RPMI 1640 supplemented with 10% (v/v) iFCS, 2 mM Glutamax, 20 mM HEPES, 50 U/mL penicillin, 50 µg/mL streptomycin, 50 µM 2-mercaptoethanol (all from Gibco®) with 200 U/mL recombinant murine granulocyte-macrophage colony-stimulating factor (GM-CSF; Peprotech)], followed by a 9-day incubation at 37°C with 5% CO_2 during which the medium was refreshed twice. After 9 days of differentiation with GM-CSF, preheated DC medium was used to recover the semi-adherent BMDC fraction which is reported to contain most CD11c+ and MHC-II^{hi} DCs [60]. Following a 10 min centrifugation at 500×*g*, cells were resuspended in DC medium and counted in PBS using a KOVA® counting chamber. Cells were then plated in a 24-well plate (1×10^6 cells/well) and incubated at 37°C with 5% CO_2.

In vitro and *in vivo* visceral *Leishmania* infections

Parasite density was assessed by counting parasites in PBS using a KOVA® counting chamber. For *in vitro* infections, cell monolayers were co-cultured with stationary-phase promastigotes of *L. infantum* at a multiplicity of infection (MOI) of 5 for a minimum of 24h at 37°C with 5% CO_2. Fixed parasites were obtained by 15 min fixation with 2% paraformaldehyde, followed by two washing steps. For *in vivo* infection, stationary-phase parasites (> 75 % metacyclics) were centrifuged for 10 min at 4,000×*g* (25°C) and resuspended to 1×10^9 parasites/mL in sterile RPMI medium. Mice were infected intravenously (i.v.) in the lateral tail vein with 1×10^8 parasites in 100µL of RPMI medium.

Paromomycin post-treatment relapse model

Mice were infected IV with 1×10^8 metacyclic promastigotes of LEM 3323 WT^{PpyRE9}. Starting from 3 days post infection (dpi), mice were treated intraperitoneally (i.p.) for 5 consecutive days with 350 mg/kg s.i.d. PMM (Sigma Aldrich).

Promastigote back-transformation

BM cells were mechanically disrupted to release the intracellular amastigotes in HOMEM promastigote medium as described by Hendrickx *et al.* [28]. At 25 °C, amastigotes readily transform back into proliferative promastigotes.

In vivo bioluminescent imaging (BLI)

Animals were monitored using *in vivo* BLI at selected time points. Imaging was performed 3 min after i.p. injection of 150 mg/kg D-Luciferin (Beetle Luciferin Potassium Salt, Promega) in the IVIS® Spectrum In Vivo Imaging System under 2.5% isoflurane inhalation anesthesia using 15 min exposure. Images were analysed using LivingImage v4.3.1 software by drawing regions of interests (ROIs) around specific organs to quantify the luminescent signal as relative luminescence units (RLU).

Phagocytosis assay

Macrophages and lineage negative BM cells were seeded at $1x10^6$ cells per well in 24-well tissue culture plates and co-cultured with live and 2% paraformaldehyde fixed parasites (LEM3323 WT$^{PpyRE9/DsRed}$) or non-fluorescent parasites (LEM3323 WT^{PpyRE9}) conjugated with 500 nM pHRodo™ Red (ThermoFisher Scientific) for two hours at 37°C with 5% CO_2 before being processed for flow cytometry.

Intracellular NO and ROS staining

To detect NO and ROS, DAF-FM Diacetate (4-amino-5-methylamino-2',7'-difluorofluorescein diacetate) and CM-H_2DCFDA were used respectively (both from ThermoFischer Scientific). Stock solutions were prepared at 5 mM in dimethyl sulfoxide (DMSO), stored at -20°C, and diluted immediately prior to use. Cells were incubated in pre-warmed PBS containing either probe in a final working concentration of 5 µM. After 30 minutes at 37°C with 5% CO_2, the loading buffer was removed, and cells were incubated for 15 minutes in dye-free medium at the same temperature to allow complete de-esterification of the intracellular diacetates. Cells were further processed for flow cytometry as described below.

Flow cytometry

Cell suspensions (2×10^7/mL concentration) were treated with Fc□R-blocking agent (anti-CD16/32, clone 2.4G2, BD Biosciences) for 15 min, followed by a washing step using 500×*g* centrifugation and resuspension in PBS + 0.2% BSA buffer. Next, cells were incubated for 20 min at 4°C with a mix of fluorescent conjugated anti-mouse antibodies (*Supplementary Table S2*) at optimized concentrations. DAPI Staining Solution (Miltenyi Biotec) was used to assess viability. Cells were measured by flow cytometry using MACSQuant® Analyzer 10 (Miltenyi Biotec) and analyses were performed using FlowLogic™ Software (Miltenyi Biotec) following specific gating strategies (*Supplementary Fig. S2, Table S1*), confirmed with fluorescence minus one (FMO) controls.

Fluorescence-activated cell sorting (FACS)

Cell suspensions were processed as above (flow cytometry) prior to cell sorting using a specific antibody mix (*Supplementary Table S2*). Cells were sorted using FACSMelody™ (BD Bioscience) following specific gating strategies, confirmed with fluorescence minus one (FMO) controls and compensated using single stains. The quality of sorting was confirmed by analyzing post-sort samples.

Epifluorescence microscopy

LT-HSCs are mainly non-adherent cells in suspension, therefore the Cytospin™ technique was employed after cell sorting to maximize cell adherence to slides prior to fluorescence staining. Both LT-HSCs and BM-derived macrophages were fixed using 2% paraformaldehyde for 15 minutes at RT, followed by two washes with PBS. Cellular cytosol (F-actin) was stained by 1h incubation with Texas Red™-X phalloidin (Thermofisher™), diluted in blocking buffer (1% BSA in PBS). Cell nuclei were counterstained with DAPI (4', 6-Diamidine-2'-phenylindole dihydrochloride) solution (Sigma®) for 2 min at RT. Finally, a drop of DABCO (1,4-Diazabicyclo[2.2.2]octane, mixture of 70% glycerol and PBS) was added and analysis was

performed using a fluorescence microscope (Zeiss Axio Observer Z1 epifluorescence microscope) with a ×63 oil objective lens and ZEN software.

Drug susceptibility determination

Use concentrations of reference drugs (PMM, Sb, MIL) were selected according to Maes *et al.* [32]. After 120 hours of drug exposure at 37°C and 5% CO_2, both LT-HSCs and BMDMs were fixed with methanol and stained with Giemsa to microscopically determine the number of intracellular amastigotes per macrophage, the percentage of infected macrophages and calculating the infection index. LT-HSCs are mainly non-adherent cells in suspension, therefore the Cytospin™ technique was employed to maximize cell adherence to slides prior to Giemsa staining. For this, slides were assembled with a slide filter card and a sample delivery chamber (all from Thermo-Shandon) and the sample (200µL of $3x10^4$ cells in RPMI medium) was loaded into the chamber. After spinning at 1000 rpm for 15 min, slides were removed from the Cytospin™ chamber and processed as above.

Quantification and statistical analysis

All statistical analyses were performed using GraphPad® Prism version 7.00 and version 9.0.1 software. Tests were considered statistically significant if $p<0.05$.

Data availability

The data that support the findings of this study are all reported in this paper and are available upon request.

Declarations

Acknowledgements

This work was supported by the Fonds Wetenschappelijk Onderzoek [www.fwo.be; grant numbers 1S30721N and G065421N] and the University of Antwerp [www.uantwerpen.be; grant number TT-ZAPBOF 33049]. The authors would like to thank Pim-Bart Feijens and Natascha Van Pelt for excellent technical assistance. LMPH is a partner of the Excellence Centre 'Infla-Med' (www.uantwerpen.be/infla-med).

Contributions

G.C. and L.M. conceived and supervised the study. G.C. and L.D. designed experiments, L.D. performed experiments, and completed the mice infection studies. L.D., S.H., L.M. and G.C. prepared the manuscript.

References

1. Burza, S., S.L. Croft, and M. Boelaert, *Leishmaniasis.* Lancet, 2018. **392**(10151): p. 951-970.
2. Ready, P.D., *Epidemiology of visceral leishmaniasis.* Clin Epidemiol, 2014. **6**: p. 147-54.

3. Kamhawi, S., *Phlebotomine sand flies and Leishmania parasites: friends or foes?* Trends Parasitol, 2006. **22**(9): p. 439-45.
4. Oliveira, F., A.M. de Carvalho, and C.I. de Oliveira, *Sand-fly saliva-leishmania-man: the trigger trio.* Front Immunol, 2013. **4**: p. 375.
5. Feijo, D., et al., *Dendritic Cells and Leishmania Infection: Adding Layers of Complexity to a Complex Disease.* J Immunol Res, 2016. **2016**: p. 3967436.
6. Martinez-Lopez, M., et al., *Leishmania Hijacks Myeloid Cells for Immune Escape.* Front Microbiol, 2018. **9**: p. 883.
7. Kedzierski, L. and K.J. Evans, *Immune responses during cutaneous and visceral leishmaniasis.* Parasitology, 2014: p. 1-19.
8. Horrillo, L., et al., *Clinical aspects of visceral leishmaniasis caused by L. infantum in adults. Ten years of experience of the largest outbreak in Europe: what have we learned?* Parasit Vectors, 2019. **12**(1): p. 359.
9. Rijal, S., et al., *Increasing failure of miltefosine in the treatment of Kala-azar in Nepal and the potential role of parasite drug resistance, reinfection, or noncompliance.* Clin Infect Dis, 2013. **56**(11): p. 1530-8.
10. Alves, F., et al., *Recent Development of Visceral Leishmaniasis Treatments: Successes, Pitfalls, and Perspectives.* Clin Microbiol Rev, 2018. **31**(4).
11. Barrett, M.P., et al., *Protozoan persister-like cells and drug treatment failure.* Nat Rev Microbiol, 2019. **17**(10): p. 607-620.
12. Tanaka, N., et al., *Use of human induced pluripotent stem cell-derived neurons as a model for Cerebral Toxoplasmosis.* Microbes Infect, 2016. **18**(7-8): p. 496-504.
13. Ferreira-da-Silva Mda, F., et al., *Primary skeletal muscle cells trigger spontaneous Toxoplasma gondii tachyzoite-to-bradyzoite conversion at higher rates than fibroblasts.* Int J Med Microbiol, 2009. **299**(5): p. 381-8.
14. Ferreira, A.V., et al., *Evidence for Trypanosoma cruzi in adipose tissue in human chronic Chagas disease.* Microbes Infect, 2011. **13**(12-13): p. 1002-5.
15. Shanks, G.D. and N.J. White, *The activation of vivax malaria hypnozoites by infectious diseases.* Lancet Infect Dis, 2013. **13**(10): p. 900-6.
16. Beamer, G., et al., *Bone marrow mesenchymal stem cells provide an antibiotic-protective niche for persistent viable Mycobacterium tuberculosis that survive antibiotic treatment.* Am J Pathol, 2014. **184**(12): p. 3170-5.
17. Pinto, A.I., et al., *TNF signalling drives expansion of bone marrow CD4+ T cells responsible for HSC exhaustion in experimental visceral leishmaniasis.* PLoS Pathog, 2017. **13**(7): p. e1006465.
18. Yarali, N., et al., *Myelodysplastic features in visceral leishmaniasis.* Am J Hematol, 2002. **71**(3): p. 191-5.

19. Abidin, B.M., et al., *Infection-adapted emergency hematopoiesis promotes visceral leishmaniasis.* PLoS Pathog, 2017. **13**(8): p. e1006422.
20. Varma, N. and S. Naseem, *Hematologic changes in visceral leishmaniasis/kala azar.* Indian J Hematol Blood Transfus, 2010. **26**(3): p. 78-82.
21. Cotterell, S.E., C.R. Engwerda, and P.M. Kaye, *Enhanced hematopoietic activity accompanies parasite expansion in the spleen and bone marrow of mice infected with Leishmania donovani.* Infect Immun, 2000. **68**(4): p. 1840-8.
22. Cotterell, S.E., C.R. Engwerda, and P.M. Kaye, *Leishmania donovani infection of bone marrow stromal macrophages selectively enhances myelopoiesis, by a mechanism involving GM-CSF and TNF-alpha.* Blood, 2000. **95**(5): p. 1642-51.
23. Liu, D. and J.E. Uzonna, *The early interaction of Leishmania with macrophages and dendritic cells and its influence on the host immune response.* Front Cell Infect Microbiol, 2012. **2**: p. 83.
24. Ali, N. and S. Hussain, *Leishmania donovani bodies in bone marrow.* Clin Case Rep, 2014. **2**(5): p. 238-9.
25. Dantas Brito, M., et al., *Visceral leishmaniasis: a differential diagnosis to remember after bone marrow transplantation.* Case Rep Hematol, 2014. **2014**: p. 587912.
26. Gawade, S., et al., *Visceral leishmaniasis: A case report.* Australas Med J, 2012. **5**(2): p. 130-4.
27. Sarkar, A., et al., *Monitoring of intracellular nitric oxide in leishmaniasis: its applicability in patients with visceral leishmaniasis.* Cytometry A, 2011. **79**(1): p. 35-45.
28. Hendrickx, S., et al., *Experimental selection of paromomycin and miltefosine resistance in intracellular amastigotes of Leishmania donovani and L. infantum.* Parasitol Res, 2014. **113**(5): p. 1875-81.
29. Ng, A.P. and W.S. Alexander, *Haematopoietic stem cells: past, present and future.* Cell Death Discov, 2017. **3**: p. 17002.
30. Boulais, P.E. and P.S. Frenette, *Making sense of hematopoietic stem cell niches.* Blood, 2015. **125**(17): p. 2621-9.
31. Walker, D.M., et al., *Mechanisms of cellular invasion by intracellular parasites.* Cell Mol Life Sci, 2014. **71**(7): p. 1245-63.
32. Maes, L., P. Cos, and S.L. Croft, *The Relevance of Susceptibility Tests, Breakpoints, and Markers*, in *Drug Resistance in Leishmania Parasites: Consequences, Molecular Mechanisms and Possible Treatments*, A. Ponte-Sucre, E. Diaz, and M. Padrón-Nieves, Editors. 2013, Springer Vienna: Vienna. p. 407-429.
33. Rishikesh, K. and K. Saravu, *Primaquine treatment and relapse in Plasmodium vivax malaria.* Pathog Glob Health, 2016. **110**(1): p. 1-8.
34. Das, B., et al., *CD271(+) bone marrow mesenchymal stem cells may provide a niche for dormant Mycobacterium tuberculosis.* Sci Transl Med, 2013. **5**(170): p. 170ra13.

35. Tornack, J., et al., *Human and Mouse Hematopoietic Stem Cells Are a Depot for Dormant Mycobacterium tuberculosis.* PLoS One, 2017. **12**(1): p. e0169119.
36. Grinenko, T., et al., *Hematopoietic stem cells can differentiate into restricted myeloid progenitors before cell division in mice.* Nat Commun, 2018. **9**(1): p. 1898.
37. Ema, H., Y. Morita, and T. Suda, *Heterogeneity and hierarchy of hematopoietic stem cells.* Exp Hematol, 2014. **42**(2): p. 74-82 e2.
38. Seita, J. and I.L. Weissman, *Hematopoietic stem cell: self-renewal versus differentiation.* Wiley Interdiscip Rev Syst Biol Med, 2010. **2**(6): p. 640-53.
39. Gomes, A.C., M. Saraiva, and M.S. Gomes, *The bone marrow hematopoietic niche and its adaptation to infection.* Semin Cell Dev Biol, 2020.
40. Pittenger, M.F., et al., *Mesenchymal stem cell perspective: cell biology to clinical progress.* NPJ Regen Med, 2019. **4**: p. 22.
41. Morrison, S.J. and D.T. Scadden, *The bone marrow niche for haematopoietic stem cells.* Nature, 2014. **505**(7483): p. 327-34.
42. Lopes, C.S., et al., *CD271+ Mesenchymal Stem Cells as a Possible Infectious Niche for Leishmania infantum.* PLoS One, 2016. **11**(9): p. e0162927.
43. Carvalho-Gontijo, R., et al., *Infection of hematopoietic stem cells by Leishmania infantum increases erythropoiesis and alters the phenotypic and functional profiles of progeny.* Cell Immunol, 2018. **326**: p. 77-85.
44. Bogdan, C., et al., *Fibroblasts as host cells in latent leishmaniosis.* J Exp Med, 2000. **191**(12): p. 2121-30.
45. Scorza, B.M., et al., *Differential Activation of Human Keratinocytes by Leishmania Species Causing Localized or Disseminated Disease.* J Invest Dermatol, 2017. **137**(10): p. 2149-2156.
46. Gangneux, J.P., et al., *In vitro and ex vivo permissivity of hepatocytes for Leishmania donovani.* J Eukaryot Microbiol, 2005. **52**(6): p. 489-91.
47. Kima, P.E., *The amastigote forms of Leishmania are experts at exploiting host cell processes to establish infection and persist.* Int J Parasitol, 2007. **37**(10): p. 1087-96.
48. Imamura, H., et al., *Evaluation of whole genome amplification and bioinformatic methods for the characterization of Leishmania genomes at a single cell level.* Sci Rep, 2020. **10**(1): p. 15043.
49. Rossi, M. and N. Fasel, *How to master the host immune system? Leishmania parasites have the solutions!* Int Immunol, 2018. **30**(3): p. 103-111.
50. Murray, H.W. and C.F. Nathan, *Macrophage microbicidal mechanisms in vivo: reactive nitrogen versus oxygen intermediates in the killing of intracellular visceral Leishmania donovani.* J Exp Med, 1999. **189**(4): p. 741-6.
51. Blos, M., et al., *Organ-specific and stage-dependent control of Leishmania major infection by inducible nitric oxide synthase and phagocyte NADPH oxidase.* Eur J Immunol, 2003. **33**(5): p. 1224-34.

52. Sousa-Franco, J., et al., *Infection-induced respiratory burst in BALB/c macrophages kills Leishmania guyanensis amastigotes through apoptosis: possible involvement in resistance to cutaneous leishmaniasis.* Microbes Infect, 2006. **8**(2): p. 390-400.
53. Roma, E.H., et al., *Impact of reactive oxygen species (ROS) on the control of parasite loads and inflammation in Leishmania amazonensis infection.* Parasit Vectors, 2016. **9**: p. 193.
54. Beltran-Povea, A., et al., *Role of nitric oxide in the maintenance of pluripotency and regulation of the hypoxia response in stem cells.* World J Stem Cells, 2015. **7**(3): p. 605-17.
55. Ludin, A., et al., *Reactive oxygen species regulate hematopoietic stem cell self-renewal, migration and development, as well as their bone marrow microenvironment.* Antioxid Redox Signal, 2014. **21**(11): p. 1605-19.
56. Nogueira-Pedro, A., et al., *Nitric oxide-induced murine hematopoietic stem cell fate involves multiple signaling proteins, gene expression, and redox modulation.* Stem Cells, 2014. **32**(11): p. 2949-60.
57. Lo Celso, C. and D. Scadden, *Isolation and transplantation of hematopoietic stem cells (HSCs).* J Vis Exp, 2007(2): p. 157.
58. Amend, S.R., K.C. Valkenburg, and K.J. Pienta, *Murine Hind Limb Long Bone Dissection and Bone Marrow Isolation.* J Vis Exp, 2016(110).
59. Dobson, K.R., et al., *Centrifugal isolation of bone marrow from bone: an improved method for the recovery and quantitation of bone marrow osteoprogenitor cells from rat tibiae and femurae.* Calcif Tissue Int, 1999. **65**(5): p. 411-3.
60. Inaba, K., et al., *Generation of large numbers of dendritic cells from mouse bone marrow cultures supplemented with granulocyte/macrophage colony-stimulating factor.* J Exp Med, 1992. **176**(6): p. 1693-702.

Figures

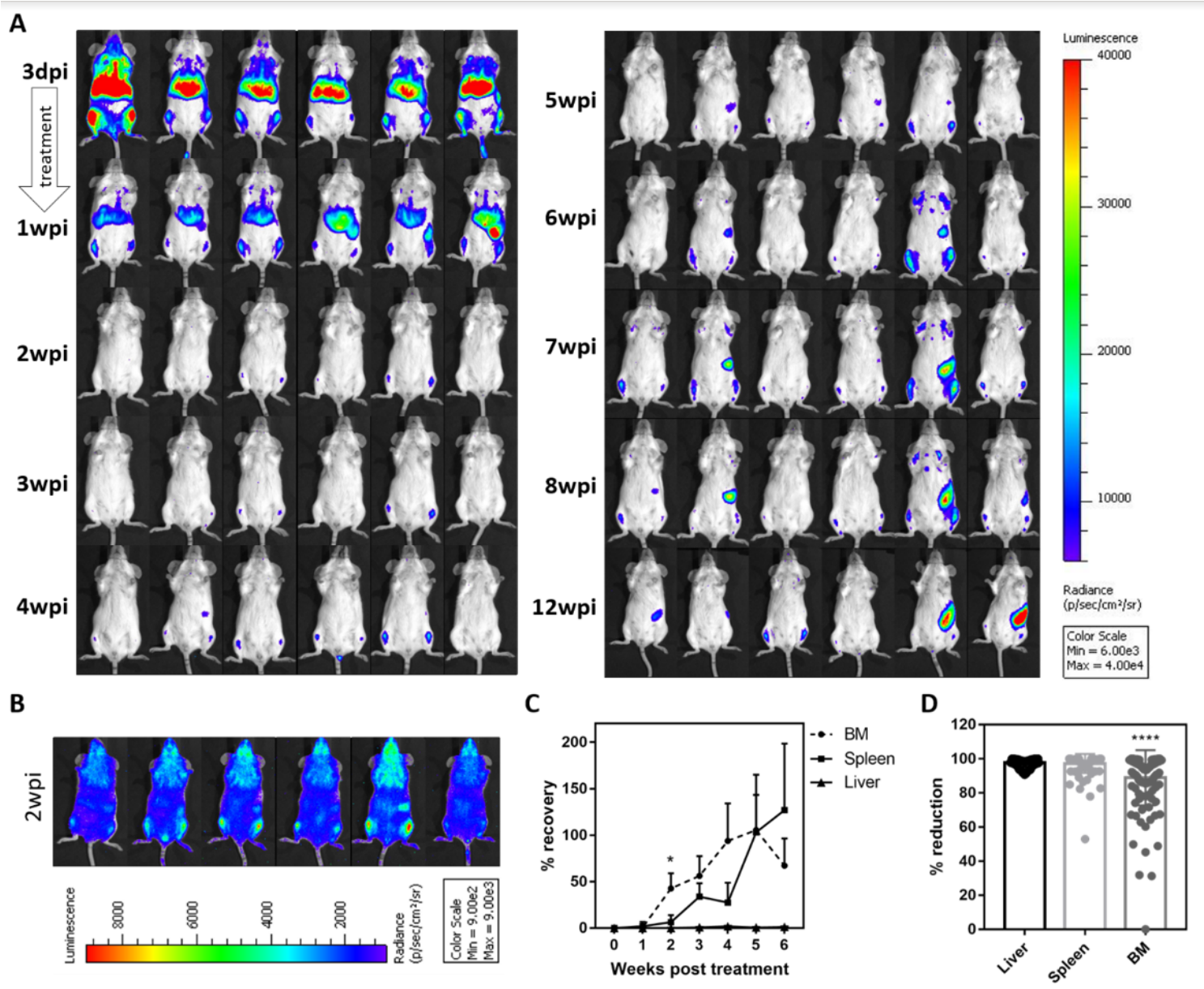

Figure 1

Reproducible post-treatment relapse model using sub-curative PMM identifies the BM as niche for treatment failure. (A) In vivo bioluminescent imaging (BLI) using an exposure time of 15 min of LEM3323 WTPpyRE9 infected BALB/c mice at 1- 12 weeks post infection (wpi) after treatment at 350 mg/kg PMM s.i.d. IP for 5 days. (B) BLI (with sensitivity scale) after 2 weeks of infection and after treatment. (C) Mean relative luminescence units (RLU) values of BM and spleen during the first 6 weeks of LEM3323 WTPpyRE9/DsRed infection in BALB/c mice, where 100% is the pretreatment RLU at 3 dpi and 0% the post-treatment RLU at 2 wpi. Results are expressed as mean ± SEM, Mann-Whitney test (two-tailed), *p≤0.05. (A-C) Groups consist of 3-6 BALB/c mice (three independent repeats). (D) Reduction in parasite burdens after treatment of Syrian Golden hamsters with a broad set (n=123) of antileishmanial test compounds; treatments with >90% clearance in the liver were considered therapeutically relevant. Wilcoxon matched-pairs signed rank test (two-tailed), ****p≤0.0001.

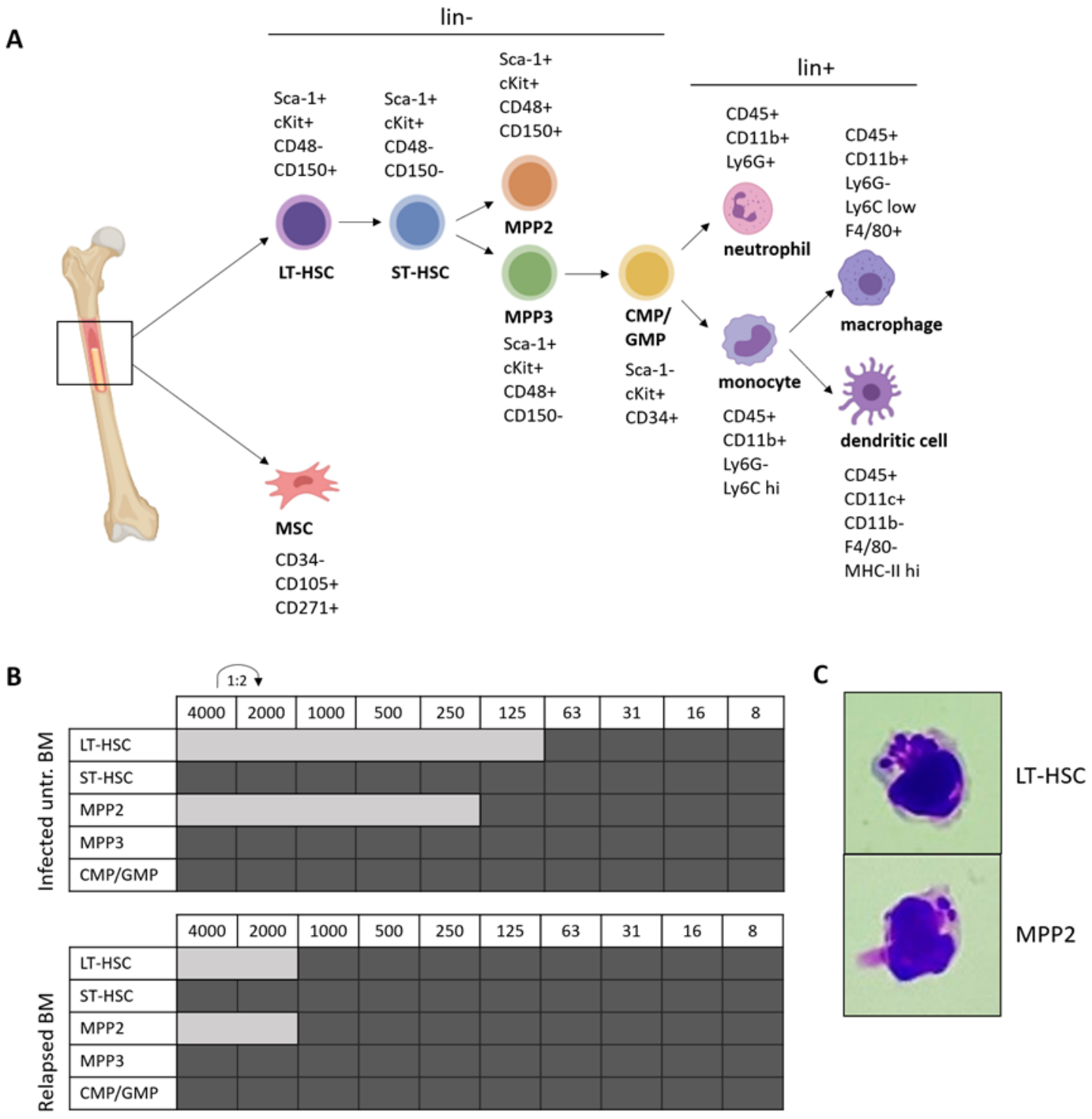

Figure 2

Identification of LT-HSCs and MPP2s as niche for viable parasites during infection and following treatment failure. (A) Specific markers for BM cell subsets: long-term hematopoietic stem cell (LT-HSC), short-term HSC (ST-HSC), multipotent progenitor (MPP), common myeloid progenitor (CMP), granulocyte-monocyte progenitor (GMP), mesenchymal stem cells (MSC). (B) Representative results of positive promastigote back-transformation after FACS of an indicated number of cells for infected untreated mice

(top panel) and relapsed mice (bottom panel) at 6 wpi. (C) Giemsa stained LT-HSC and MPP2 cells sorted from LEM3323 WTPpyRE9/DsRed infected BALB/c mice.

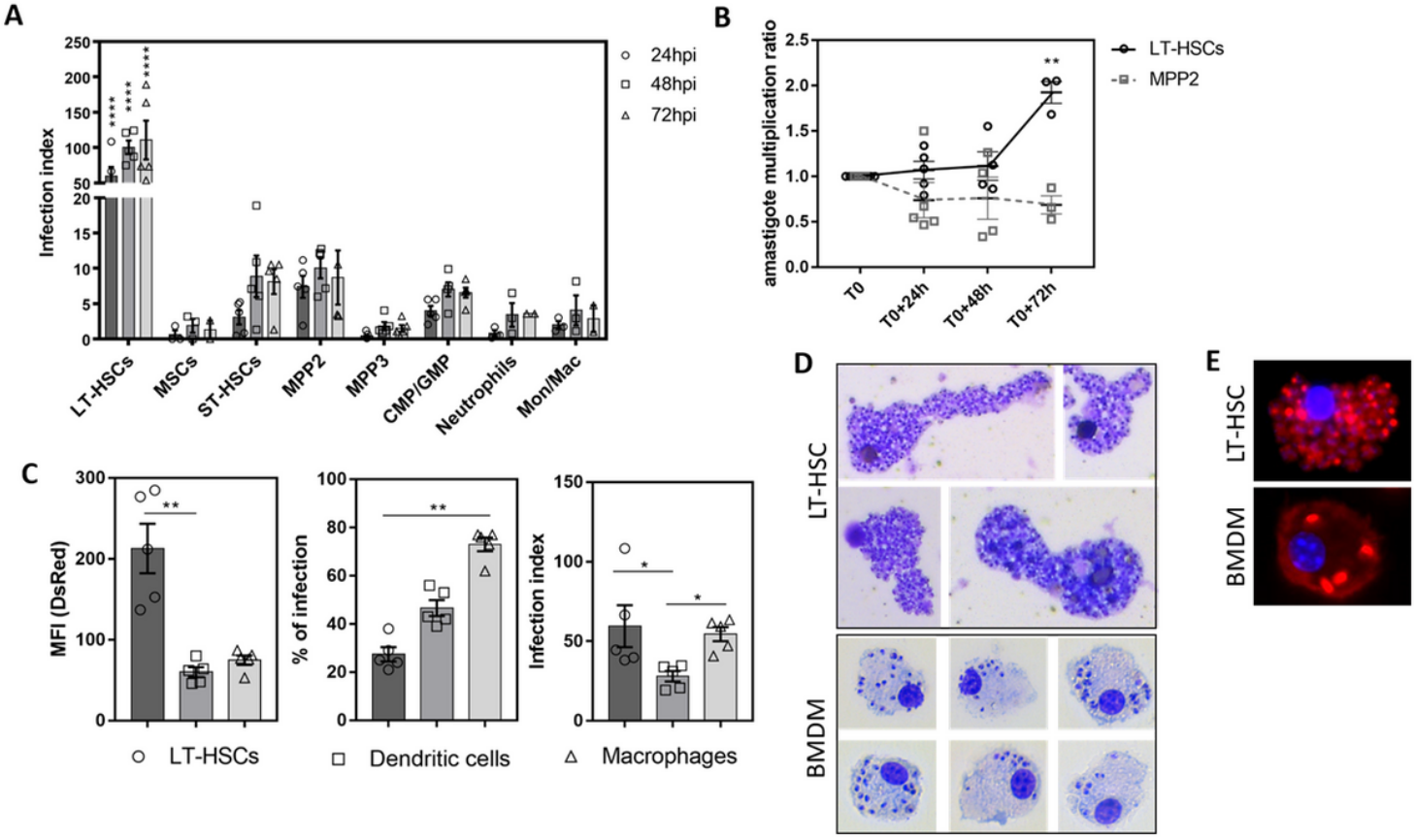

Figure 3

LT-HSCs are most susceptible to VL infection ex vivo. (A) Ex vivo LEM3323 WTPpyRE9/DsRed infection of lineage depleted BM collected from BALB/c mice: infection index representing DsRed MFI × % of infection. (B) Evolution over time of the DsRed MFI indicating intracellular parasite expansion (amastigote multiplication ratio) in two BM cell subsets: LT-HSCs and MPP2s. (C) Comparison of MFI, % infection and infection index between BM-derived dendritic cells and macrophages and LT-HSCs, (D) Giemsa staining of LEM3323 WTPpyRE9/DsRed infected BM-derived macrophages and sorted LT-HSC, (E) Immunofluorescence staining of (D) with nuclei stained with DAPI (blue) and F-actin with Texas-RedTM-X Phalloidin (red). (A-C) Days post-infection (dpi), median fluorescence intensity (MFI), mesenchymal stem cell (MSC), long-term hematopoietic stem cell (LT-HSC), short-term hematopoietic stem cell (ST-HSC), multipotent progenitor (MPP), common myeloid progenitor (CMP), granulocyte-monocyte progenitor (GMP), monocyte/macrophage (Mon/Mac), (D-E) bone marrow derived macrophages (BMDM). Results are shown as mean ± SEM and are based on at least three independent repeats ($3 \leq n \leq 5$). Statistical significance was found with two-tailed tests, i.e. 2way ANOVA in (A), Kruskal-Wallis in (C), and multiple t test in (D). *p<0.05, **p<0.01, ****p<0.0001.

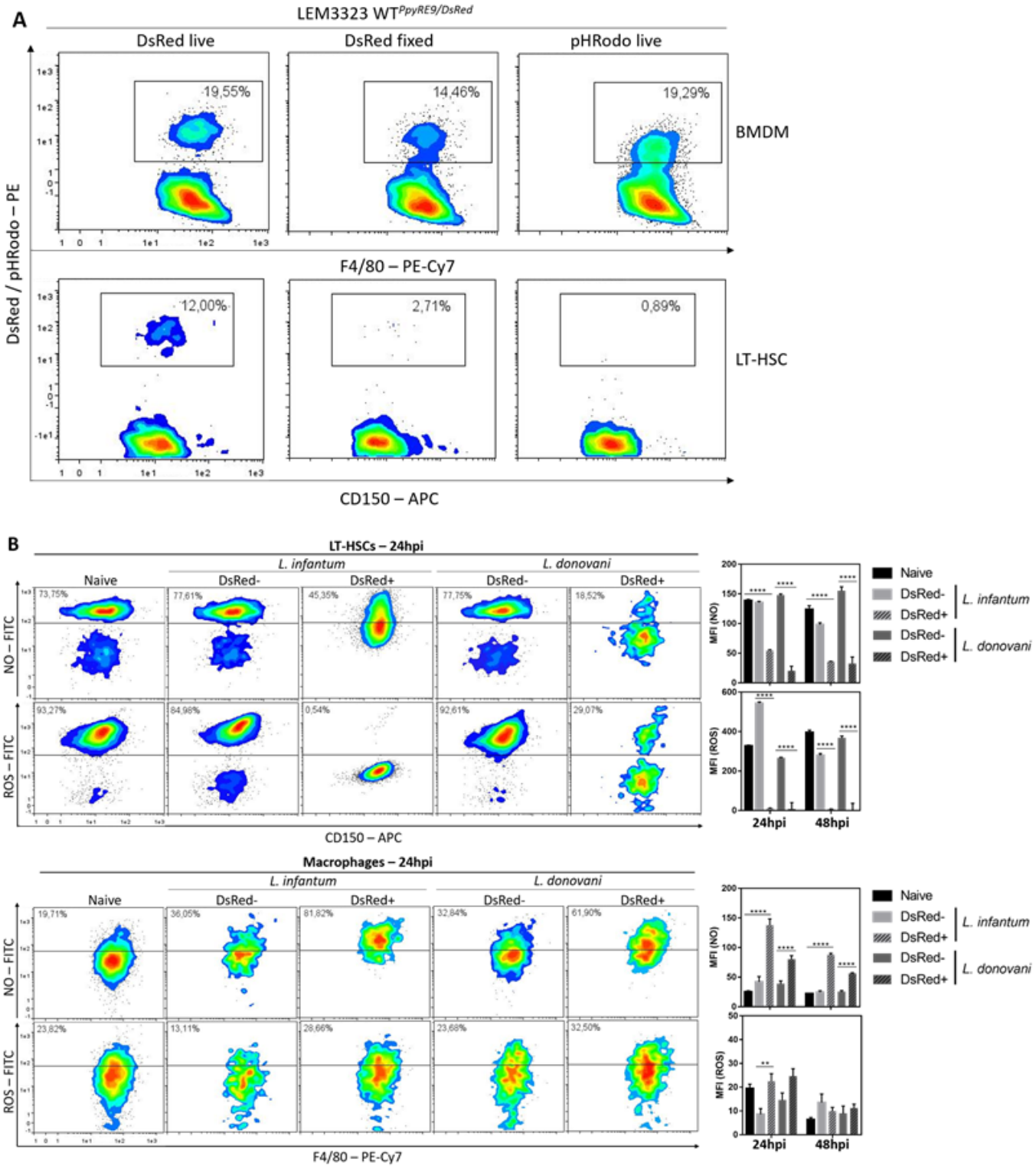

Figure 4

Leishmania infects LT-HSCs by parasite entry and suppresses NO and ROS levels. (A) Density plots of BM-derived macrophages (BMDM, top panel) and Lin- cKit+ Sca-1+ CD48- CD150+ LT-HSC (lower panel) after a 2-hour incubation with live or 2% paraformaldehyde fixed LEM3323 WTPpyRE9/DsRed parasites. Right panels correspond to cells infected with pHrodo Red labeled LEM3323 WTPpyRE9 parasites. Representative plots of two independent repeats are shown. (B) ROS and NO levels, determined using CM-

H2DCFDA and DAF-FM Diacetate, are decreased in ex vivo infected stem cells. Density plots of LT-HSCs (top panel) and BMDMs (bottom panel) at 24 h post infection (hpi) with fluorescent signal of NO (top rows) and ROS (bottom rows). Graph represents the MFI of these plots, adding 48 h post-infection. Representative plots, with corresponding graphs, of three independent repeats with similar results are shown. Multiple t tests (two-tailed), 155 ≤ n ≤ 16250, **p<0.01, ****p<0.0001.

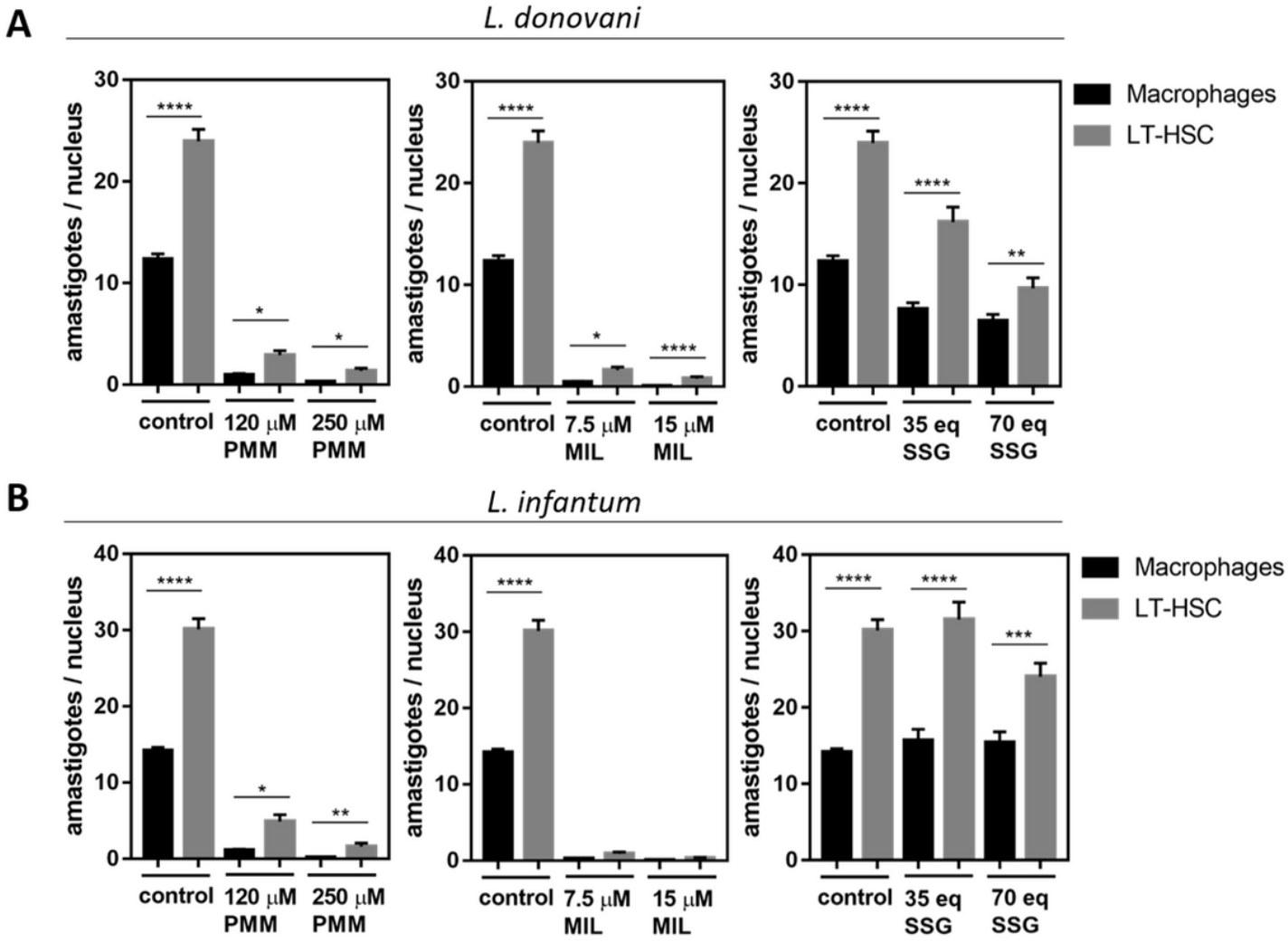

Figure 5

Infected LT-HSC are less sensitive to antileishmanial drug action compared to infected macrophages. (A) Sorted LT-HSCs infected with L. donovani Ldl82 WTPpyRE9/DsRed in a 5:1 ratio and treated for 120h. Representative plots of two independent repeats for PMM (120 μM and 250 μM), MIL (7.5 μM and 15 μM) and SSG (35 eq Sb and 70 eq Sb) are shown. (B) Confirmatory results with PMM, MIL and SSG on L. infantum LEM3323 (with inherent Sb resistance) in two independent repeats. Mann-Whitney test, 45 ≤ n ≤ 250, *p<0.05, **p<0.01, ****p<0.0001.

Supplementary Files

This is a list of supplementary files associated with this preprint. Click to download.

- Supplementary.docx